Biochemical Journal (2021) **478** 2571–2587
https://doi.org/10.1042/BCJ20210295

Research Article

The interplay of self-assembly and target binding in centrin 1 from *Toxoplasma gondii*

Carolina Conter[1,*], Luca Bombardi[1,*], Marco Pedretti[1], Filippo Favretto[1], Adele Di Matteo[2], Paola Dominici[1] and Alessandra Astegno[1]

[1]Department of Biotechnology, University of Verona, Strada Le Grazie 15, 37134 Verona, Italy; [2]Institute of Molecular Biology and Pathology, CNR, Piazzale Aldo Moro, 5, 00185 Rome, Italy

Correspondence: Alessandra Astegno (alessandra.astegno@univr.it)

Centrins are conserved calcium (Ca^{2+})-binding proteins typically associated with centrosomes that have been implicated in several biological processes. In *Toxoplasma gondii*, a parasite that causes toxoplasmosis, three centrin isoforms have been recognized. We have recently characterized the metal binding and structural features of isoform 1 (TgCEN1), demonstrating that it possesses properties consistent with a role as a Ca^{2+} sensor and displays a Ca^{2+}-dependent tendency to self-assemble. Herein, we expanded our studies, focusing on the self-association and target binding properties of TgCEN1 by combining biophysical techniques including dynamic light scattering, isothermal titration calorimetry, nuclear magnetic resonance, circular dichroism, and fluorescence spectroscopy. We found that the self-assembly process of TgCEN1 depends on different physicochemical factors, including Ca^{2+} concentration, temperature, and protein concentration, and is mediated by both electrostatic and hydrophobic interactions. The process is completely abolished upon removal of the first 21-residues of the protein and is significantly reduced in the presence of a binding target peptide derived from the human XPC protein (P17-XPC). Titration of P17-XPC to the intact protein and isolated domains showed that TgCEN1 possesses two binding sites with distinct affinities and Ca^{2+} sensitivity; a high-affinity site in the C-lobe which may be constitutively bound to the peptide and a low-affinity site in the N-lobe which is active only upon Ca^{2+} stimulus. Overall, our results suggest a specific mechanism of TgCEN1 for Ca^{2+}-modulated target binding and support a N-to-C self-assembly mode, in which the first 21-residues of one molecule likely interact with the C-lobe of the other.

Introduction

Centrins are highly conserved calcium (Ca^{2+})-binding proteins that are widely distributed throughout the eukaryote kingdom. They were initially identified in green algae as components of Ca^{2+}-sensitive contracting fibers [1–3]. Later, centrins were found in the centrosome-like microtubule-organizing centers (MTOCs) in many other organisms [2,4–6]. However, increasing evidence establishes that centrins localize not only to centrosomes but also to other cell compartments and organelles [7]. These different localizations have been shown to be essential to the functions of centrin in various biological processes, such as DNA repair, centrosome duplication, mRNA nuclear export, and signal transduction [8–13].

Centrins possess a structural organization similar to the prototype Ca^{2+}-binding protein calmodulin (CaM) with the presence of two independent domains, namely the N- and the C-terminal domains which are linked by an α-helix; each domain contains two helix-loop-helix motifs, called the EF-hands, which contain potential Ca^{2+}-binding sites. Ca^{2+} binding to the EF-hand motifs controls an important conformational change from a closed to an open state, exposing the hydrophobic surface for the interaction of the protein with its signaling partners [10,14].

*These authors contributed equally to this work.

Received: 28 April 2021
Revised: 9 June 2021
Accepted: 11 June 2021

Accepted Manuscript online: 11 June 2021
Version of Record published: 9 July 2021

Biochemical Journal (2021) **478** 2571–2587
https://doi.org/10.1042/BCJ20210295

Toxoplasma gondii, an apicomplexan parasite responsible for toxoplasmosis, possesses three centrin isoforms, i.e. centrin 1 (TgCEN1), centrin 2 (TgCEN2), and centrin 3 (TgCEN3) [15]. Recent studies in our laboratory demonstrated that TgCEN1 behaves biochemically as a Ca^{2+} sensor *in vitro*, being able to bind two Ca^{2+} ions via its N-terminal EF-hands and to undergo significant Ca^{2+}-dependent conformational changes that result in the exposure of hydrophobic surfaces [16]. Thus, as a regulatory protein, the biological function of TgCEN1 should be mediated by interaction with downstream proteins. However, until now, no reports regarding its physiological targets and cellular functions have been published. TgCEN1 is highly similar to human centrin 1 (HsCEN1) and centrin 2 (HsCEN2) (~70% identity). Sequence alignment of centrins from different organisms indicated that the higher variability occurs mainly within the first 20–25 residues of the N-terminal region, which has no counterpart in CaM, and has been suggested to be responsible for Ca^{2+}-dependent self-assembly and polymerization of centrins [14,17–20]. Experimental data on centrins from yeast, green algae, ciliate, and humans demonstrated that they can form multimers and suggested that centrins have important structural functions by contributing to the formation of Ca^{2+}-sensitive contractile filaments [14,17–19]. Our previous work has shown that TgCEN1 is also able to reversibly self-assemble in the presence of Ca^{2+} and has demonstrated the importance of the N-terminal fragment (preceding the first EF-hand motif) in this process [16]. Notably, TgCEN1 mainly localizes to centrioles/centrosomes [15], and therefore it may also be involved in the formation of supramolecular assemblies.

Herein, we expanded the information on the macromolecular properties of TgCEN1 by better investigating the self-assembly process of the protein and its dependence on different physicochemical factors, and by characterizing the energetics and structural features of the interaction of TgCEN1 with a peptide derived from the human xeroderma pigmentosum group C protein (P17-XPC), which is a well-known natural target of centrins [21]. To this end, we have used a comprehensive approach combining different biophysical techniques including dynamic light scattering (DLS), isothermal titration calorimetry (ITC), nuclear magnetic resonance (NMR), circular dichroism (CD), and fluorescence spectroscopy. Cloning and expression of the two isolated N- and C-terminal domains (N-TgCEN1, 1–94 aa and C-TgCEN1, 95–169 aa) and comparison of the results for the entire protein provided further information to probe the biochemical behavior of the protein. Our results support a finely tuned regulation of TgCEN1 with respect to the self-association propensity and the interaction with specific targets that depends on Ca^{2+} concentration and other physicochemical factors, providing insights into the possible structural and regulatory roles of TgCEN1 in the dynamics of centrosomes.

Materials and methods

Protein production and peptide synthesis

The full-length TgCEN1 and the truncated variant of TgCEN1 lacking the first 21 residues (Δ21TgCEN1) were overexpressed in *E. coli* strain Rosetta and purified as described previously [16].

The N- and C-terminal domains of TgCEN1 were produced by recombinant techniques. The N-domain (N-TgCEN1, 1–94 aa) and its variant lacking the first 21 residues (Δ21N-TgCEN1, 22–94 aa) were obtained by the introduction of a termination codon at the position coding for Ala95 of both the intact TgCEN1 and truncated Δ21TgCEN1 forms using the QuikChange® site-directed mutagenesis kit (Agilent Technologies). The primers used to introduce the amino acid substitution were as follows: forward (5′-catgactgtcaagatgtgag aacgcgatccgcgcg-3′) and reverse (5′-cgcgcggatcgcgttctcacatcttgacagtcatg-3′). The C-domain (C-TgCEN1, 95–169 aa) was obtained introducing a Tobacco Etch Virus (TEV) cleavage site after Met94 using the following primers: forward (5′-gactgtcaagatggaaaaccttttatttccagggtgcagaacgcgatc-3′) and reverse (5′-gatcgcgttctgcaccct ggaaataaaggttttccatcttgacagtc-3′). Both domains were efficiently expressed in *E. coli* strain Rosetta and purified via Nickel affinity chromatography. Incubation with a previously prepared recombinant His-tagged TEV-protease was carried out for 16 h at 4°C (ratio 1 : 50). Tag-free proteins were reloaded into a His-trap column and collected in the flow-through. Protein concentration was determined using the Biuret method [22] and purity of the proteins was confirmed by SDS–PAGE to be at least 90%. Purified proteins were washed in 50 mM Tris–HCl, 150 mM KCl, pH 7.5 and protein aliquots were stored at −80°C until use.

To produce ^{15}N-labelled proteins for NMR analysis, cells were grown in M9 minimal medium with $^{15}NH_4Cl$ (1 g L^{-1}) as a sole nitrogen source.

The P17-XPC peptide (847-NWKLLAKGLLIRERLKR-863) and N21 peptide (1-MHSRKGASSLPRG RGAGKKTE-21) were purchased from GenScript U.S.A. Inc. (NJ, U.S.A.). The peptides purity was estimated higher than 90% by HPLC and their molecular mass was verified by electrospray ionization mass spectrometry

(ESI-MS). P17-XPC peptide concentration was calculated using its predicted molar extinction coefficient ($\varepsilon_0 280 = 5500\ M^{-1}\ cm^{-1}$, http://web.expasy.org/protparam/).

Turbidimetry

Turbidity experiments were conducted on a Jasco V-560 UV-visible spectrophotometer by recording absorbance at 340 nm as a function of time with 1 cm path length quartz cuvettes. Standard conditions were 20 mM Tris–HCl, 20 mM KCl pH 7.5, protein concentration of 20 μM, 1 mM $CaCl_2$ at 37°C. The effects of different physicochemical parameters on the self-assembly propensity of TgCEN1 and its domains were assessed by varying the $CaCl_2$ concentrations (0–2 mM), temperature (4–45°C), protein concentrations (5–50 μM), and salt concentrations (0–150 mM KCl). The turbidity changes were also monitored in the presence of 1-anilino-8-naphthalenesulphonic acid (ANS) at a final concentration of 600 μM.

Dynamic light scattering

Dynamic Light Scattering (DLS) measurements were done on a Zetasizer Nano ZS instrument (Malvern Instruments, Worcestershire, U.K., 4 mV He-Ne laser, $l_0 = 633$ nm, $q = 173°$) equipped with a Peltier temperature controller, using disposable 12.5 × 45 mm cells with stopper to prevent evaporation [23]. Protein samples (200 μl of 10 μM protein, except where differently specified) in 20 mM Tris–HCl, 20 mM KCl pH 7.5 were clarified by centrifugation (21 000 *g* for at least 30 min) before starting acquisition to remove debris. All buffers were filtered immediately before measurements. The diameter of particles, describing their macromolecular size in solution, was reported as number distribution to emphasize the relative proportions of species of different sizes.

In the thermal ramping experiment, sample aliquots (200 μl of 5 μM protein in the presence of 1 mM $CaCl_2$) were introduced into the temperature-controlled sample compartment and the temperature was ramped from 15 to 45°C with 1°C increments, with size measurements collected at every 1°C increase. Data were reported as *z*-average which is the intensity weighted mean hydrodynamic size of the collection of particles. Transition midpoint (T_m) of the process was obtained by fitting the signal changes to a logistic curve.

Far-UV circular dichroism spectroscopy

Circular dichroism (CD) measurements were carried out with a Jasco J-1500 spectropolarimeter equipped with a Peltier type thermostated cell holder. Far-UV spectra (200–250 nm) were an average of five accumulations recorded at 25°C with the same parameters as previously described [13,24]. Protein and peptide concentrations were 10–20 μM in 0.1 cm quartz cuvettes. CD spectra were recorded in 50 mM Tris–HCl, 150 mM KCl pH 7.5, 0.5 mM DTT in the presence of an excess of $CaCl_2$ or EGTA with respect to the protein concentration. The spectrum of the buffer alone was subtracted from that of the sample.

Fluorescence spectroscopy

Fluorescence spectra were recorded on a Jasco FP8200 spectrofluorimeter. The binding of TgCEN1 or its domains to P17-XPC peptide was followed by monitoring the fluorescence of the single Trp residue of the peptide [12,25,26]. Excitation was set at 295 nm and fluorescence emission was measured from 305 to 500 nm, with 5 nm excitation and emission bandwidths. The buffer used was 50 mM Tris–HCl, 150 mM KCl pH 7.5, 0.5 mM DTT, in the presence of 5 mM $CaCl_2$ or 5 mM EGTA.

Isothermal titration calorimetry

Isothermal titration calorimetry (ITC) experiments were conducted on a MicroCal PEAQ-ITC (Malvern) instrument. The proteins and peptides were solubilized in the same buffer containing 50 mM Tris–HCl, 150 mM KCl pH 7.5 and 5 mM $CaCl_2$ or 5 mM EGTA, which was filtered and degassed before each run. Typical ITC measurements were performed by titrating 30–50 μM of protein (0.2 ml) with a 1 or 1.5 μl injection of 0.5 mM peptide at 25°C (total injections 39 or 26, respectively) with an injection interval of 120 or 180 s.

An injection of peptide into buffer without any protein was considered as reference and subtracted from each experiment. The first injection (0.2 μl) was ignored in the final data analysis. Titrations were analyzed by a two or one-site peptide-binding model. The best fitting was used to get apparent dissociation constants (K_d) and enthalpy changes (ΔH), as previously described [27]. The reported thermodynamic parameters are the

Biochemical Journal (2021) 478 2571–2587
https://doi.org/10.1042/BCJ20210295

mean ± standard error of the mean (SEM) of at least three independent titrations using two different protein preparations.

Nuclear magnetic resonance spectroscopy

Nuclear magnetic resonance spectroscopy (NMR) experiments were performed at 298 K on a 600 MHz Bruker Avance III spectrometer, equipped with a triple resonance cryo-probe. ^{15}N-labelled protein was dissolved in 50 mM Tris–HCl, 50 mM KCl pH 7.5, 0.5 mM DTT, 10% D_2O at a final concentration of ∼0.4 mM. The ^{15}N-labeled protein was gradually titrated with a $CaCl_2$ solution to a final concentration of 5 mM. Successively, the Ca^{2+}-bound ^{15}N-labeled protein was titrated with increasing amounts of unlabeled P17-XPC, dissolved in the same NMR buffer, until reaching a final molar ratio protein : peptide of 1 : 2.5. Complex formation was monitored acquiring both ^{1}H-^{15}N-SOFAST-HMQC (heteronuclear multiple quantum coherence) experiments [28] and ^{1}H-^{15}N HSQC (heteronuclear single quantum coherence) spectra before and after each addition of P17-XPC. Both experiments were recorded with a data matrix of 2048 (F2,1H) × 256 (F1,15N) complex points and spectral windows of 8417.51 Hz (1H) × 1642.06 Hz (15N) [29]. In total, eight transients were acquired with a recycle delay of 1.2 s and 0.2 s for the ^{1}H-^{15}N HSQC and the ^{1}H-^{15}N-SOFAST-HMQC experiments, respectively. The NMR spectra were processed using Topspin v. 3.6.2 (Bruker) and NMRpipe[30], while data analysis and spectra investigation were performed with the software Ccpnmr Analysis v. 2.5.2 [31].

Results

Self-assembly process of TgCEN1 depends on different physicochemical factors

In our previous work, we demonstrated that TgCEN1 has a high tendency to self-assemble in the presence of Ca^{2+} [16]. The self-assembly tendency of TgCEN1 was followed by monitoring light scattering at 340 nm as a function of time at 37°C and using 20 μM protein concentration (Figure 1A). Upon addition of Ca^{2+} (1 mM) TgCEN1 displayed a clear increase in turbidity, while, in the absence of Ca^{2+} (i.e. in the presence of the metal chelator EGTA) it did not (Figure 1A). Moreover, upon addition of EGTA to Ca^{2+}-saturated TgCEN1, the turbidity at 340 nm was significantly reduced and the sample regained optical transparency, supporting a reversible Ca^{2+}-dependent process (Figure 1A) [16].

To distinguish the species present in solution in the turbidity experiments, new DLS studies were undertaken under the same conditions (37°C, 20 mM Tris–HCl, 20 mM KCl pH 7.5). DLS is a powerful tool to study the formation of molecular assembly in solution and to obtain information on the relative size distributions of protein assemblies. Scattering spectra were recorded for 10 μM solutions of TgCEN1 in the absence and presence of 1 mM Ca^{2+}. In the absence of Ca^{2+}, DLS spectra of TgCEN1 displayed a single narrow peak, corresponding to particles with number-averaged hydrodynamic diameter of 7.54 ± 0.01 nm (Figure 1B), which is compatible with a single prevailing monomeric form of the protein. Interestingly, upon addition of Ca^{2+} this peak disappeared, and a new distinct species appeared with a diameter of 570 ± 5 nm (Figure 1B). In this case, the Gaussian distribution was wider with respect to that observed in the absence of Ca^{2+}, indicating a heterogeneous distribution of particle size. A deeper analysis of Ca^{2+} dependence of TgCEN1 self-assembly indicated that a moderate molar excess of Ca^{2+} was required to initiate the association process. As shown in Figure 1C the intensity of the scattered light, measured as turbidity at 340 nm after 25 min, increased as a function of Ca^{2+} concentration and had a plateau at high Ca^{2+} concentrations. A 7.5 : 1 metal/protein ratio was the minimum where light scattering was detected. No changes in the turbidity profiles were observed upon Mg^{2+} addition (up to 10 mM, data not shown), suggesting that the association process is Ca^{2+} specific. These results clearly confirm the Ca^{2+}-dependent reversible ability of TgCEN1 to associate and form larger scattering objects.

Self-assembly properties of TgCEN1 were also analyzed as a function of temperature and protein concentration. Increasing the temperature resulted in an increase in the slope of the growth phase at 340 nm and a higher plateau indicative of a faster self-assembly process and of the larger size of the scattering particles, respectively (Supplementary Figure S1A). Accordingly, DLS analysis showed that the mean diameter of TgCEN1 particles varied significantly as a function of temperature. The increase in temperature resulted in the increase in the *z*-average hydrodynamic diameter of TgCEN1 particles (from ∼230 nm at 15°C to ∼470 nm at 45°C) with a transition midpoint at 36 ± 1°C (Figure 1D). As for the temperature, the increase in TgCEN1 concentrations also caused a faster self-assembly process and a higher plateau (Supplementary Figure S1B). Low

Biochemical Journal (2021) **478** 2571–2587
https://doi.org/10.1042/BCJ20210295

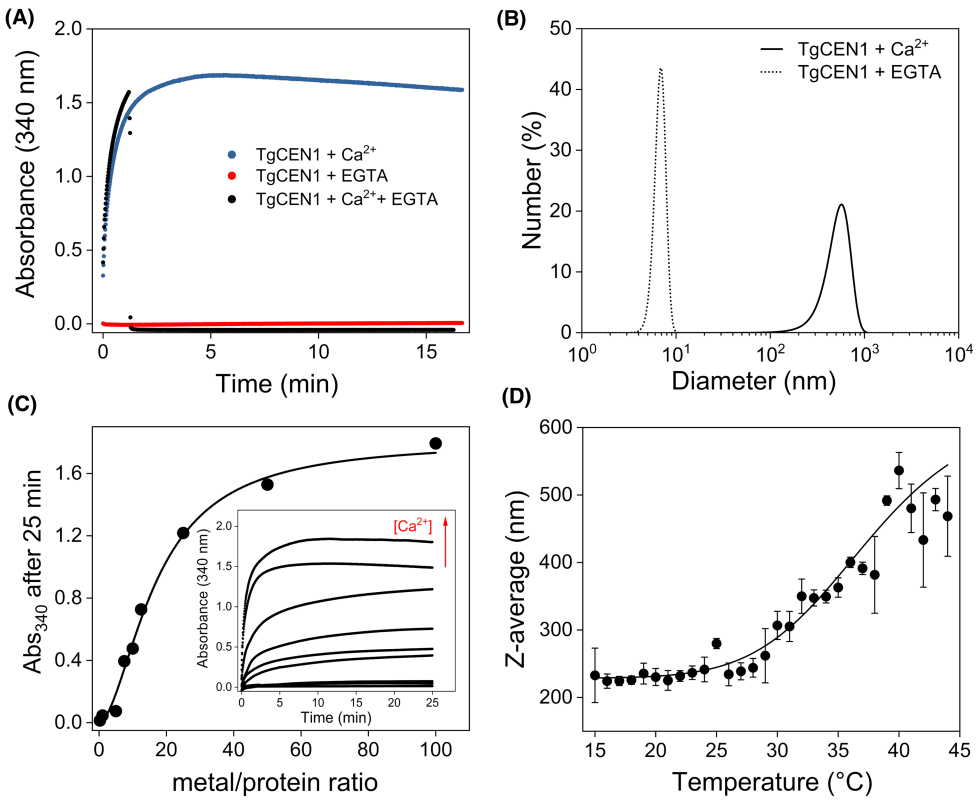

Figure 1. Self-assembly properties of TgCEN1.

(**A**) Turbidity measurements of TgCEN1. Scattering intensity (measured as the turbidity at 340 nm) of TgCEN1 as a function of time at 37°C in 20 mM Tris–HCl, 20 mM KCl pH 7.5 protein concentration of 20 μM, in the presence of 1 mM EGTA (red) or 1 mM $CaCl_2$ (blue). The effect of EGTA on a solution of Ca^{2+}-saturated TgCEN1 is also shown (black). (**B**) Particle-size distribution from DLS data of 10 μM TgCEN1 in 20 mM Tris–HCl, 20 mM KCl pH 7.5 at 37°C in the presence of 1 mM EGTA (dotted line) or 1 mM $CaCl_2$ (solid line). (**C**) Dependence of the TgCEN1 self-assembly on the Ca^{2+}concentrations. *Main*, turbidity (at 340 nm after 25 min) is represented as a function of metal/protein ratio. *Inset,* Turbidity profiles of 20 μM TgCEN1 (measured at 340 nm) as a function of time at increasing Ca^{2+}concentrations (5, 20, 100, 150, 200, 250, 500, 1000, and 2000 μM). (**D**) Effects of temperature on TgCEN1 particles hydrodynamic diameter. Best fit of the experimental data is represented as a black line.

light scattering was observed at protein concentrations less than 5 μM, supporting the existence of a threshold concentration for the occurrence of the self-assembly process.

To understand the nature of the forces driving TgCEN1 association, we next examined self-assembly of TgCEN1 by varying the ionic strength of the solution (0–150 mM KCl). A clear inhibition of self-assembly process at high ionic strength was seen, supporting the contribution of electrostatic interactions in self-assembly. As shown by turbidity profiles (Figure 2A), at low salt concentration the reaction was very fast, and an increase in ionic strength is accompanied by a progressive decrease in the assembly rate (decrease in the slope of the growth phase) and in the intensity of the final plateau. Consistently, the DLS number distribution indicated a dominant particle population with a hydrodynamic diameter of ∼7 nm at high ionic strength, while at low salt concentrations species with larger diameters (600–800 nm) are prevalent (Figure 2B).

Along with electrostatic interactions, hydrophobic forces are also crucial in protein self-assembly. Thus, to study the involvement of a hydrophobic component in self-association of TgCEN1, we used the fluorescent probe ANS which offers a spectroscopic approach to assess hydrophobicity of the protein's surface. We found that the binding of ANS interferes with the assembly process. As shown in Figure 2C, the final intensity of the scattered light, measured as turbidity at 340 nm, decreased at increasing ANS concentrations. This inhibition effect suggests that the binding sites of ANS at least partially overlap with the interacting regions involved in

Biochemical Journal (2021) **478** 2571–2587
https://doi.org/10.1042/BCJ20210295

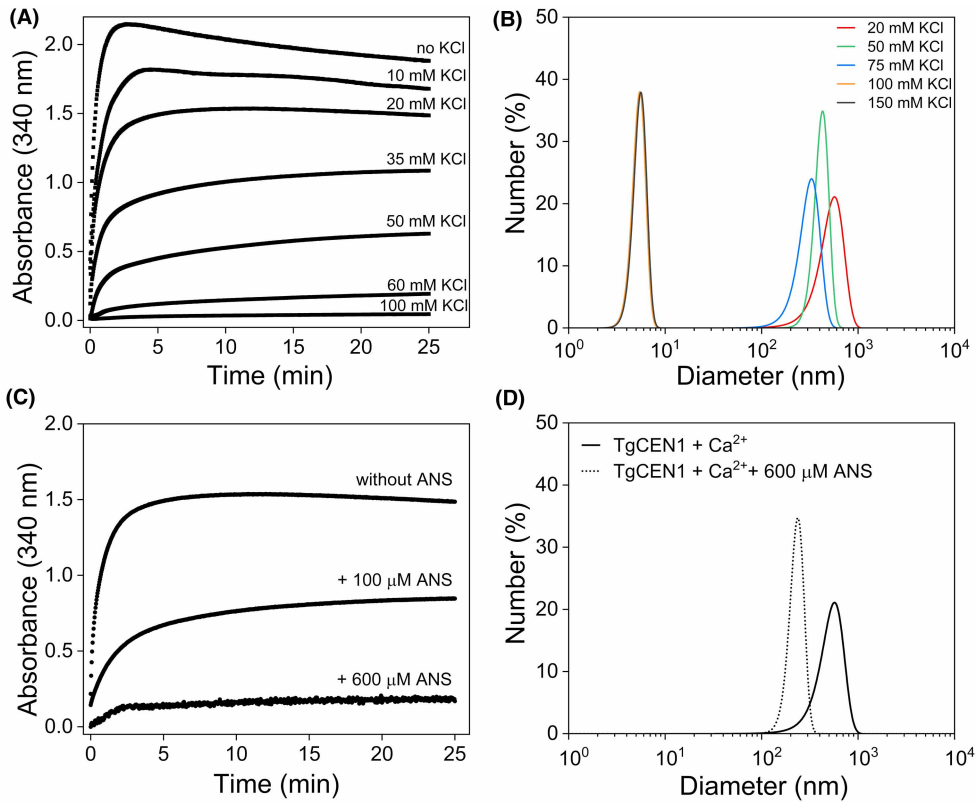

Figure 2. Effects of ionic strength and ANS on TgCEN1 self-assembly.

(**A** and **B**) Dependence of the TgCEN1 self-assembly on KCl concentrations. (**A**) Turbidity profiles and (**B**) particle-size distribution from DLS data of TgCEN1 in 20 mM Tris–HCl pH 7.5 at different KCl concentrations in the presence of 1 mM $CaCl_2$, at 37°C. (**C** and **D**) Inhibitory effect of ANS. (**C**) Turbidity profiles and (**D**) particle-size distribution from DLS data of TgCEN1 in 20 mM Tris–HCl, 20 mM KCl pH 7.5, 1 mM $CaCl_2$, at 37°C in the absence and presence of ANS.

self-association; thus, ANS binding likely hampers aggregation by shielding TgCEN1 hydrophobic regions involved in the assemblies. Of note, no complete disappearance of light scattering was observed even at high concentrations of ANS, indicating that the association process was not completely quenched by the addition of ANS. Accordingly, the hydrodynamic diameter of TgCEN1 particles decreased upon addition of ANS (from ∼570 nm in the absence of ANS to ∼238 nm in the presence of 600 μM ANS), although a complete conversion of TgCEN1 assemblies to the monomeric form did not occur (Figure 2D). Together, these results suggest both hydrophobic and electrostatic contributions to the self-assembly process.

Contribution of protein domains to the self-assembly process

Similar to CaM, centrins are composed of an N- and C-terminal lobe separated by a flexible linker region (an α-helix or a short loop). However, centrins are unique in possessing an additional N-terminal positively charged tail of ∼20–25 residues with variable composition that is usually disordered. In TgCEN1, this region encompasses the first 21 residues, has a basic character (three Lys and three Arg, +5 net charge), and exhibits a high intrinsic disorder based on GeneSilico MetaDisorder Service analysis [32]. Previous experiments in our laboratory using a truncated variant of TgCEN1 lacking the first 21 residues (Δ21TgCEN1) support the notion that the N-terminal portion in centrins has a role in the self-association process. Indeed, no changes in turbidity at 340 nm were observed upon addition of 1 mM Ca^{2+} to Δ21TgCEN1 sample under the same experimental conditions used for the full-length protein (Supplementary Figure S2A) [16]. Accordingly, new DLS measurements showed the presence of a single peak centered at 7.01 ± 0.01 nm compatible with a monomeric protein in both the absence and presence of Ca^{2+} (Supplementary Figure S2B). No changes in turbidity or size distribution were observed for the Δ21TgCEN1 variant under all the other conditions tested in the present work

(temperature, protein concentration, KCl, and ANS) (Supplementary Figure S2). Thus, the Ca^{2+}-dependent self-assembly process is completely abolished upon removal of the first 21 residues of the protein, highlighting that this basic portion is essential for TgCEN1 assemblies.

To explore the hypothesis that the N-terminal fragment can mediate Ca^{2+}-modulated heterologous interactions between N- and C-lobes belonging to two different subunits, we synthesized a peptide comprising the first N-terminal 21 residues of TgCEN1 (N21, Met1-Glu21) and analyzed its effects on the Δ21TgCEN1 variant that does not self-assemble. As shown by the turbidity experiments (Figure 3A), the peptide alone did not aggregate upon addition of Ca^{2+} in solution. On the other hand, when the peptide was added to the Δ21TgCEN1, an increase in the light scattering at 340 nm was observed. Accordingly, in the presence of N21 peptide, Δ21TgCEN1 showed an increase in hydrodynamic radius (from 7.01 ± 0.01 nm to 485 ± 3 nm) (Figure 3B) as well as in DLS count rate (which constitutes the average scattering intensity in the measurement, Supplementary Figure S3).

We also investigated the contribution of the individual N- and C-lobe of TgCEN1 to the self-assembly process, by cloning the isolated N- and C-terminal domains (N-TgCEN1, 1–94 aa; C-TgCEN1, 95–169 aa) and analyzing their association propensity under different experimental conditions. The two domains were well-folded in the presence of 1 mM Ca^{2+}, as suggested by their far-UV CD spectra (Supplementary Figure S4A). Interestingly, even if they exhibited no turbidity changes at 340 nm upon addition of Ca^{2+} (Supplementary Figure S4B), DLS analysis revealed the presence of particles with diameter of 250 ± 1 nm for N-TgCEN1 and 311 ± 1 nm for C-TgCEN1, respectively (Supplementary Figure S4C). An inhibition of association process was observed for the N-TgCEN1 at high ionic strength with a shift of the particle size towards smaller size

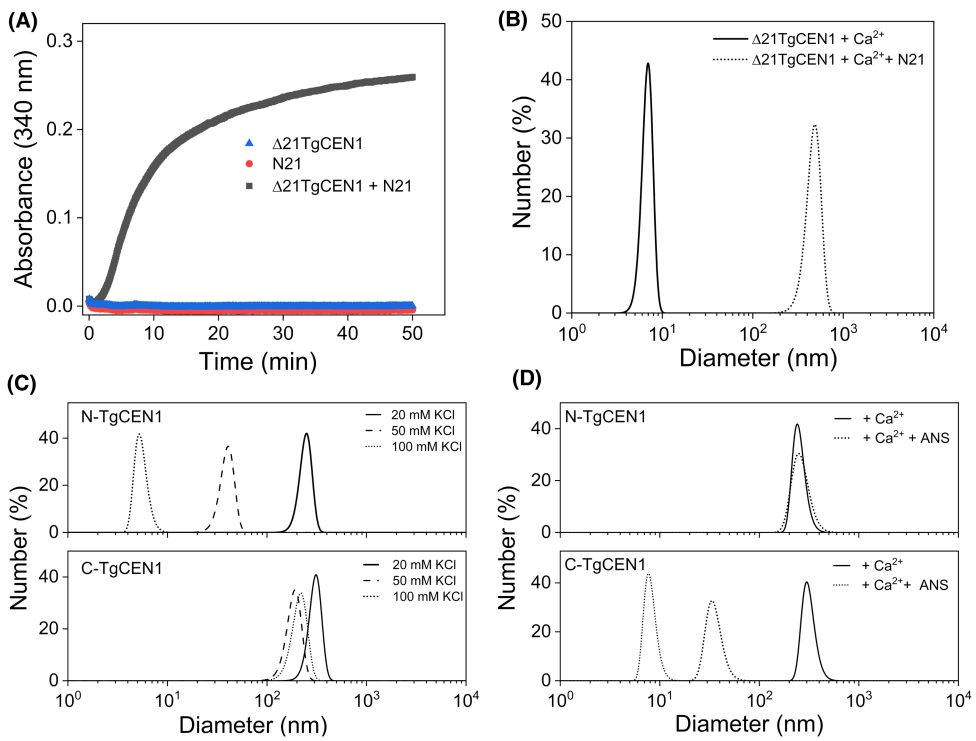

Figure 3. Contribution of protein domains to self-assembly.

(**A**) Scattering intensity (measured as the turbidity at 340 nm) of 20 μM Δ21TgCEN1 as a function of time at 37°C in 20 mM Tris–HCl, 20 mM KCl pH 7.5 before (blue line) and upon (black line) addition of 50 μM N21 peptide in the presence of 1 mM $CaCl_2$. The profile of N21 peptide alone in the presence of 1 mM $CaCl_2$ is also shown (red line). (**B**) Particle-size distribution from DLS data of 10 μM Δ21TgCEN1 in 20 mM Tris–HCl, 20 mM KCl pH 7.5 at 37°C before (solid line) and upon (dotted line) addition of 50 μM N21 peptide in the presence of 1 mM $CaCl_2$. (**C** and **D**) Particle-size distribution from DLS data of 10 μM N-TgCEN1 and C-TgCEN1 in 20 mM Tris–HCl pH 7.5 in the presence of 1 mM $CaCl_2$ at selected KCl concentrations (**C**) and upon addition of 600 μM ANS (**D**).

Biochemical Journal (2021) 478 2571–2587
https://doi.org/10.1042/BCJ20210295

following the increase in salt concentration, while only small changes in the DLS profiles of C-TgCEN1 were observed (Figure 3C). On the other hand, the addition of ANS had no effect on N-TgCEN1 but had a remarkable impact on the association properties of C-TgCEN1, causing a decrease in diameters of the particles in solution (new species with diameters of 35 ± 1 nm and 7.96 ± 0.01 nm) (Figure 3D).

Taken together, these data suggest that the two N and C isolated domains of TgCEN1 also have an aggregation propensity that is mediated mainly by electrostatic forces for the N-terminal domain and by hydrophobic forces for the C-terminal domain. However, the entire protein is required for TgCEN1 to self-assemble into larger oligomers, most likely attributable to heterologous interactions between N- and C-terminal domains of different molecules mediated by the basic N-terminal 21 residues.

TgCEN1 has a specific Ca^{2+}-controlled target binding mechanism

Our previous studies demonstrated that, upon binding Ca^{2+}, TgCEN1 exposed a hydrophobic area which is likely instrumental for the interaction with target proteins [16]. The physiological targets of TgCEN1 are not known at present, although it is well-established that the centrin targets in many organisms usually have a typical binding motif consisting of the hydrophobic triad W^1L^4 L^8 (1–4–8 motif) [33–35]. We therefore used ITC to study the energetics of the interaction of TgCEN1 and its isolated N- and C-terminal domains with a 17-residue target peptide derived from the nucleotide excision repair human xeroderma pigmentosum group C protein (P17-XPC). This peptide represents a high affinity human centrin binding site which is in the C-terminal portion of XPC (between residues N847 and R863) and exhibits the hydrophobic triad (W848, L851 and L855) [33]. To avoid experimental artifacts and misinterpretations associated with the abovementioned self-assembly propensity of full-length TgCEN1, for the binding experiments we used the truncated variant of TgCEN1 lacking the first 21 residues (Δ21TgCEN1, 22–169) and the N-terminal domain lacking the first 21 residues (Δ21N-TgCEN1, 22–94 aa).

Representative isotherms for P17-XPC binding to Δ21TgCEN1 and the individual domains in the presence of Ca^{2+} or EGTA are shown in Figure 4 and the thermodynamic parameters are presented in Table 1. The ITC experiments showed that in the presence of Ca^{2+} the binding of P17-XPC to Δ21TgCEN1 is exothermic. The binding curve is clearly characterized by a two-step process, which best fit to a model predicting two sets of sites: one high-affinity site (K_{d1} of 1.3 ± 0.3 nM) and a second site with lower affinity (K_{d2} of 4.1 ± 0.9 μM) (Figure 4A and Table 1). On the other hand, in the absence of Ca^{2+}, the thermogram showed a single interaction site with a K_d of 59.1 ± 11.8 nM (Figure 4B and Table 1). These results were confirmed by studying the binding of each isolated lobe to the peptide. Calorimetric titrations of P17-XPC to C-TgCEN1 showed a single binding event (stoichiometry of 1) with similar affinity both in the presence and in the absence of Ca^{2+} (K_d of 6.7 ± 1.1 nM with Ca^{2+} and K_d of 50.1 ± 9.7 nM without Ca^{2+}), indicating that the complex formation between the peptide and the C-terminal domain is not significantly influenced by Ca^{2+} availability (Figure 4C,D and Table 1). It is worth mentioning that the K_d values obtained for the binding of P17-XPC to the C-TgCEN1 are very similar to that of the high affinity site in the intact protein, thus implying that the high affinity site in holo-Δ21TgCEN1 corresponds to the C-terminal domain. Interestingly, the N-terminal domain displayed a single binding site with a K_d of ∼0.4 μM only in the presence of Ca^{2+}, while no measurable binding affinity was obtained with the apo-Δ21N-TgCEN1 (Figure 4E,F and Table 1), clearly suggesting that the sole binding site in the apo-protein is located in the C-lobe.

Further insight into the TgCEN1 target recognition mode was obtained by examining the interaction of Ca^{2+}-bound ^{15}N-labeled Δ21TgCEN1 with the P17-XPC peptide through ^{15}N-HSQC titration experiments. As evident in Figure 5A, several ^1H-^{15}N resonances, dispersed throughout the HSQC spectrum, undergo significant chemical shift perturbation in presence of peptide, suggesting that a strong conformational rearrangement of the holo-protein is induced by binding of P17-XPC. The ^{15}N-HSQC titrations again pointed to two P17-XPC binding sites on Ca^{2+}-bound Δ21TgCEN1 with different affinities. Up to a 1 : 1 stoichiometric ratio, the binding is described by slow chemical exchange, which is usually associated to binding events characterized by a high affinity [36], as the $^1H(N)$ backbone resonances corresponding to Ca^{2+}-bound protein gradually disappear without a significant line broadening (i.e. peak 4, Figure 5B) and those for complexed-protein appear (i.e. peaks 1 and 2, Figure 5B). On the other hand, the binding of the second peptide caused a relevant line broadening and change in positioning of some ^1H-^{15}N cross-peaks (i.e. peaks 3, 5, G43 and G79, Figure 5B). This effect is a distinctive mark of cross-peaks undergoing an intermediate exchange on an NMR timescale and is indicative of a substantially weaker affinity for this interaction (K_d in the μM range) [37]. The types of chemical exchange found for the two binding events agree well with the affinities obtained by calorimetry.

Biochemical Journal (2021) **478** 2571–2587
https://doi.org/10.1042/BCJ20210295

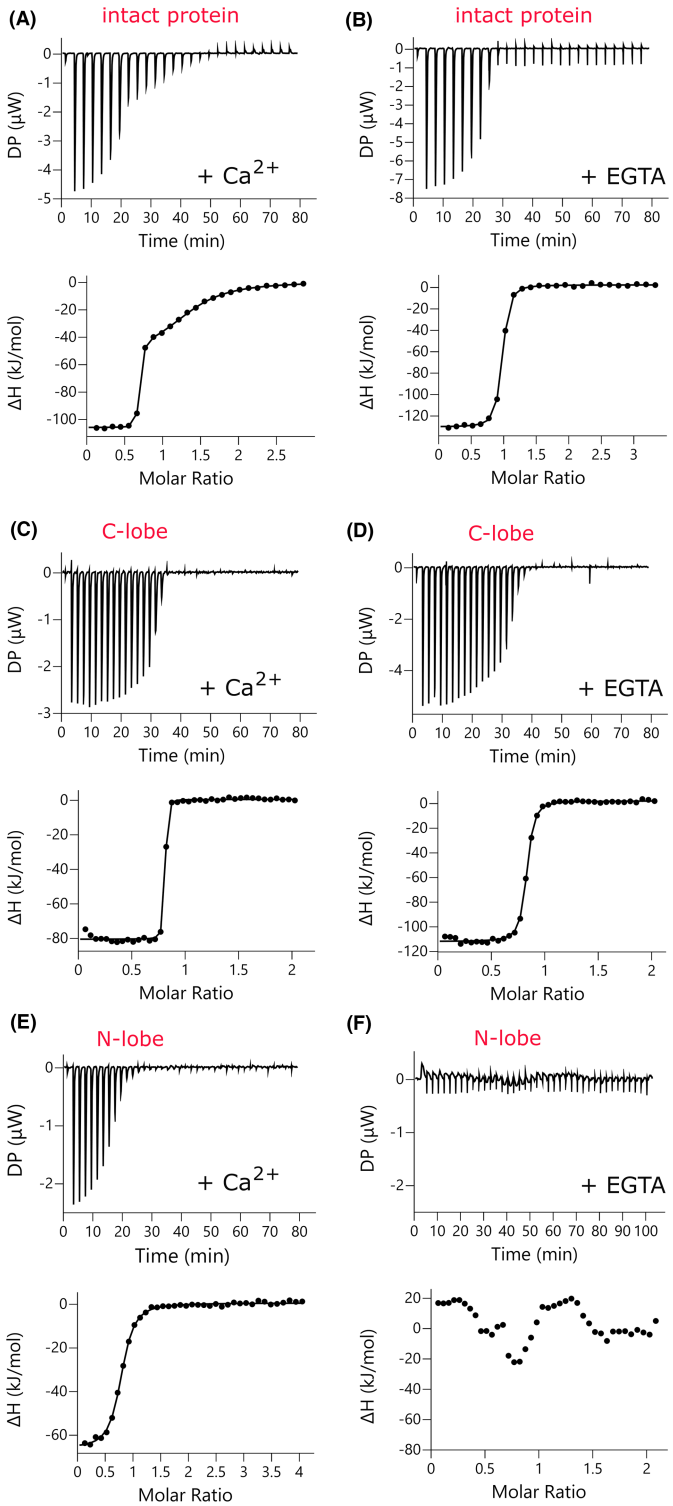

Figure 4. P17-XPC binding to Δ21TgCEN1 and its N- and C-terminal domains studied by ITC in the presence and absence of Ca^{2+}.

Representative thermograms (top panels) and the derived binding isotherms (bottom panels) of titration of P17-XPC into Δ21TgCEN1 (**A** and **B**), C-TgCEN1 (**C** and **D**), and Δ21N-TgCEN1 (**E** and **F**) in the presence of 5 mM $CaCl_2$ or 5 mM EGTA at 25°C. The ligand dilution blank experiments (P17-XPC titrated into buffer) were subtracted from the binding isotherm obtained in the presence of protein. A first injection of 0.2 µl was made and then the first data point was removed from data fitting.

PORTLAND PRESS

Biochemical Journal (2021) **478** 2571–2587
https://doi.org/10.1042/BCJ20210295

Table 1 Thermodynamic parameters of the interaction of Δ21TgCEN1 and its N- and C-terminal domains with P17-XPC in the presence of 5 mM $CaCl_2$ or 5 mM EGTA at 25°C

	Buffer condition	n	K_d (nM)	ΔH (kJ mol^{-1})	−TΔS (kJ mol^{-1})
Δ21TgCEN1 + P17-XPC	$CaCl_2$	$n_1 = 0.7 \pm 0.1$	1.3 ± 0.3	−99.7 ± 5.3	48.6 ± 5.8
		$n_2 = 0.8 \pm 0.1$	4102 ± 914	−50.8 ± 11.3	25.7 ± 11.5
	EGTA	0.9 ± 0.1	59.1 ± 11.8	−131.7 ± 1.6	89.9 ± 1.9
Δ21N-TgCEN1 + P17-XPC	$CaCl_2$	0.7 ± 0.1	396.3 ± 60.9	−74.25 ± 4.3	37.4 ± 3.9
	EGTA	-	-	-	-
C-TgCEN1 + P17-XPC	$CaCl_2$	0.8 ± 0.1	6.7 ± 1.1	−95.7 ± 9.9	48.8 ± 10.2
	EGTA	0.8 ± 0.1	50.1 ± 9.7	−118.7 ± 2.9	76.5 ± 3.1

The reported parameters are the mean ± standard error of the mean (SEM) of at least three independent titrations using two different protein preparations.

Interestingly, the resonances corresponding to two N-terminal glycines, G43 and G79 of Δ21TgCEN1, which were previously assigned [16], seem to be almost unperturbed up to a 1 : 0.5 protein : peptide molar ratio, while a dramatic signal decrease and line broadening at 1 : 1 stoichiometric ratio were observed (Figure 5, green asterisk). Above a 1 : 1 ratio, we could observe a significant chemical shift change and sharpening of these resonances. At 2.5 molar excess of P17-XPC, the second binding site is completely saturated. Our NMR data suggest that the two glycine residues are likely involved in the binding of the second peptide or are reporters of a second event of binding, thus supporting the hypothesis that the low affinity site is located in the N-terminal domain.

Additional evidence that in the apo-TgCEN1 a single binding site for the P17-XPC is located on the C-lobe was obtained by fluorescence spectroscopy, monitoring the Trp residue (W848) of the P17-XPC. Addition of stoichiometric amount of both holo- and apo-C-TgCEN1 to the P17-XPC solution resulted in a blue shift in maximum wavelength and an increase in fluorescence intensity of Trp, confirming that Trp848 of the peptide

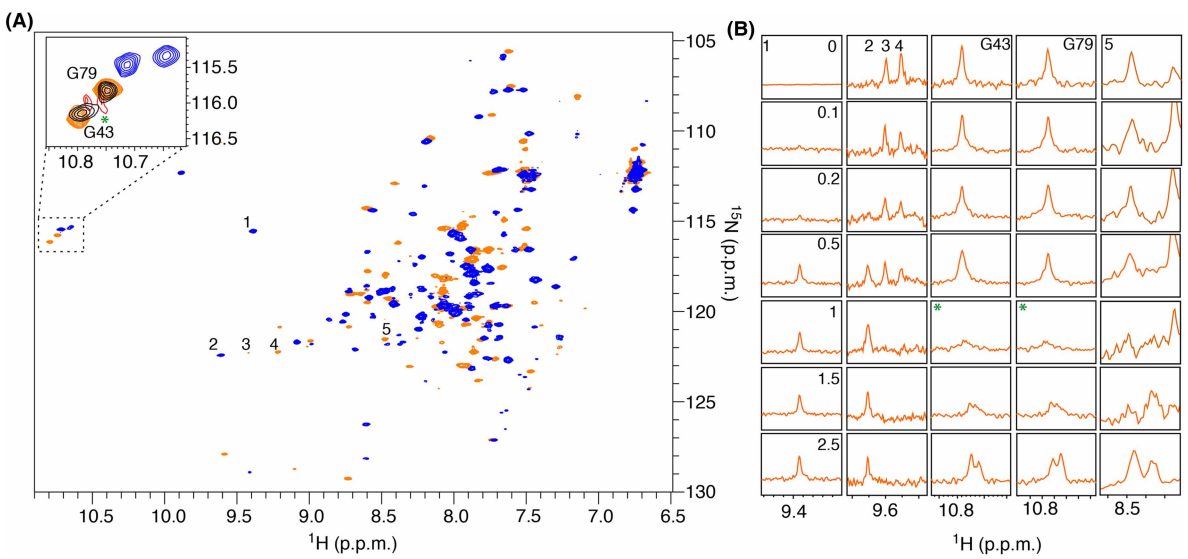

Figure 5. ^{15}N-HSQC titrations spectra of the binding of P17-XPC to ^{15}N-labeled Ca^{2+}-Δ21TgCEN1.
(**A**) ^{15}N-HSQC spectra of ^{15}N-labeled Δ21TgCEN1 in its Ca^{2+}-bound conformation collected at titration steps corresponding to the [peptide]/[protein] molar ratio of 0 (orange) and 2.5 (blue). The magnified region of G43 and G79 is shown in the panel. Selected titration points collected at titration steps corresponding to the [peptide]/[protein] molar ratio of 0 (orange), 0.5 (black), 1 (red) and 2.5 (blue) are reported. The asterisk highlights the beginning of the saturation of the second binding site corresponding to a [peptide]/[protein] molar ratio of 1. (**B**) One dimensional ^{1}H-traces of selected peaks of the ^{1}H-^{15}N HSQC spectrum of ^{15}N-labeled Δ21TgCEN1 shown in **A** in the presence of increasing concentration of P17-XPC. [peptide]/[protein] molar ratios are reported in the panel corresponding to peak 1.

is involved in binding to C-TgCEN1 both in the apo and holo-state (Supplementary Figure S5). Stoichiometric addition of the N-lobe to the peptide in the presence of Ca^{2+} paralleled what observed for the C-lobe (blue shift and Trp fluorescence emission increment), while no changes in the fluorescence spectrum of P17-XPC upon addition of the N-lobe in the presence of EGTA were observed (Supplementary Figure S5).

Altogether, the ITC, NMR and fluorescence data indicated that TgCEN1 has two sites for the binding of target peptide P17-XPC: one high-affinity site in the C-lobe which displays poor Ca^{2+} sensitivity and one low-affinity site in the N-lobe which binds the peptide in a Ca^{2+}-dependent manner.

Thermodynamic parameters of the binding between P17-XPC with the entire TgCEN1 and its N- and C-terminal domains obtained by ITC analysis suggested that this process is driven by an enthalpic component, which compensates for the unfavorable entropy (Table 1). This negative entropy may be associated with a conformational rearrangement following formation of the complex. To investigate this point, we carried out far-UV CD analysis. As shown in Figure 6, the isolated Δ21N- and C-TgCEN1 domains are well-folded with spectral properties that are indicative of protein containing mainly α-helical structure (two minima at 208 and 222 nm); on the contrary, free P17-XPC in the aqueous solution displayed a spectrum with an ellipticity close to zero as expected for an unfolded peptide. Upon addition of stoichiometric amounts of P17-XPC to C-TgCEN1 an increase in the ellipticity of the bands at 208 and 222 nm was observed which reveals an increase in the α-helixes both in the presence of Ca^{2+} or not (i.e. with EGTA), and confirms an interaction between the peptide and the C-lobe even in the absence of Ca^{2+} (Figure 6A). Since the free peptide has a predominantly random coil conformation and generally the EF-hand containing proteins do not increase their helical content after binding to their target peptides [12,13,24,38–42], the higher ellipticity signal observed for the bimolecular complex could be ascribed to induced helicity in P17-XPC upon binding to C-TgCEN1 (as suggested by the difference spectra where the CD spectrum of C-TgCEN1 alone is subtracted from that of the complex). The same changes in CD profiles were obtained for the N-lobe in the presence of Ca^{2+}, but not upon peptide addition to the apo-domain (Figure 6B), therefore supporting the hypothesis that the binding of P17-XPC to the N-lobe of TgCEN1 is Ca^{2+}-dependent.

Target peptide binding has an inhibitory effect on the self-assembly process of TgCEN1

To get insight into the interplay between self-assembly and target binding we investigated the effect of P17-XPC on the Ca^{2+}-induced association of TgCEN1. As suggested by turbidity measurements at 340 nm, the addition of the peptide clearly inhibited the self-assembly process in the intact TgCEN1 (Figure 7A). Accordingly, the hydrodynamic radius of TgCEN1 particles decreased upon addition of P17-XPC (from 570 ± 5 nm to 307 ± 1 nm) (Figure 7B). These results agree with previous observations on the centrins from

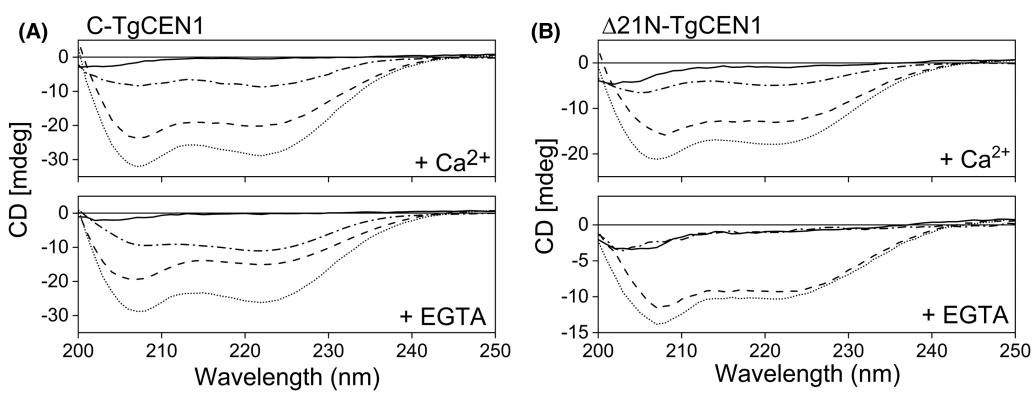

Figure 6. Far UV CD analysis of P17-XPC binding to isolated domains.

(**A**) Far UV CD spectra of 20 μM P17-XPC alone (solid line), 20 μM C-TgCEN1 (dashed line), and 1 : 1 protein–peptide complex (dotted line) in the presence of 5 mM $CaCl_2$ (top) or EGTA (bottom). (**B**) Far UV CD spectra of 20 μM P17-XPC alone (solid line), 20 μM Δ21N-TgCEN1 (dashed line), and 1 : 1 protein–peptide complex (dotted line) in the presence of 5 mM $CaCl_2$ (top) or EGTA (bottom). The CD spectrum resulting from subtraction of the spectrum of protein–peptide complex from that of protein alone was also shown (dash-dotted line).

Biochemical Journal (2021) **478** 2571–2587
https://doi.org/10.1042/BCJ20210295

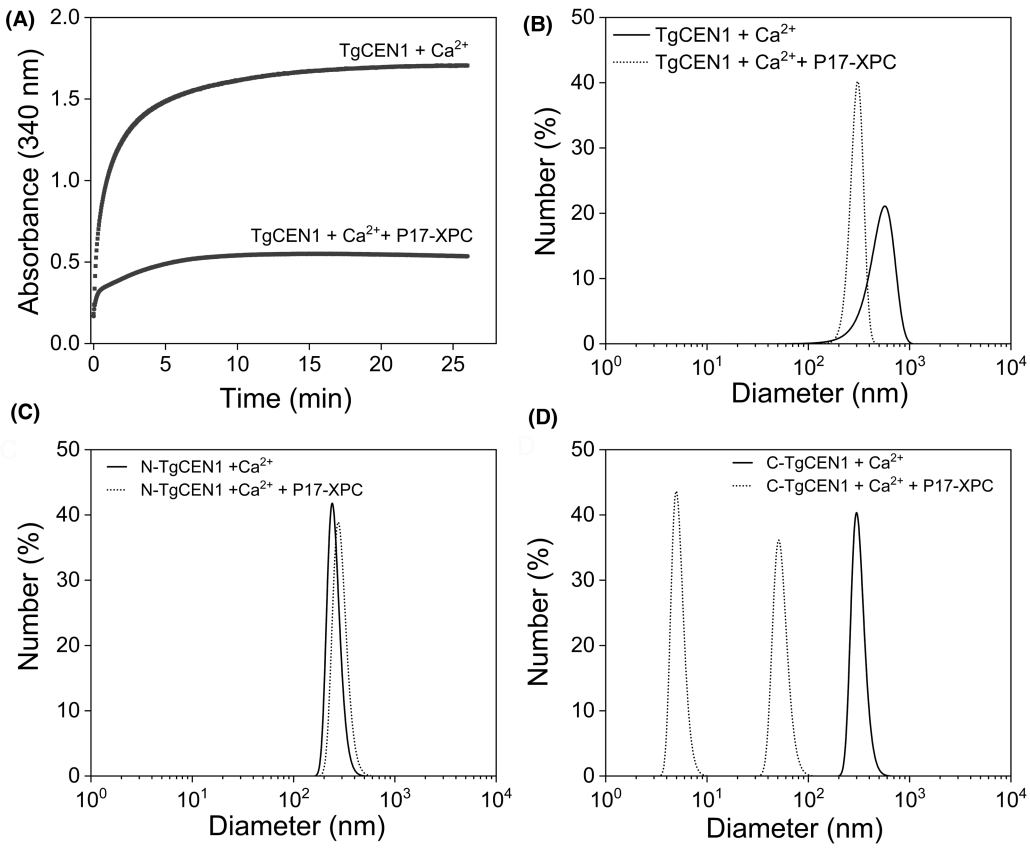

Figure 7. Inhibitory effect of P17-XPC on TgCEN1 self-assembly.

(**A**) Turbidity profiles of intact TgCEN1 and (**B** and **D**) particle-size distribution from DLS data of (**B**) intact TgCEN1, (**C**) N-TgCEN1 and (**D**) C-TgCEN1 in 20 mM Tris–HCl, 20 mM KCl pH 7.5, 1 mM $CaCl_2$, at 37°C in the absence and presence of P17-XPC.

S. cerevisiae (Cdc31p), *S. dubia* (SdCEN), HsCEN1 and HsCEN2 for which the presence of the binding peptide Kar1p (centrosomal target protein) caused a strong reduction in the formation of multimeric structures [14] and with the observation that addition of XPC peptide to centrin from *Euplotes octocarinatus* (EoCEN) resulted in the dissociation of protein aggregates [43].

Of note, addition of P17-XPC to N-TgCEN1 had no effect on the association properties of this domain. The DLS distributions showed the presence of the same species in both the absence and presence of the peptide (Figure 7C). On the other hand, the peptide had a remarkable impact on assembly of C-TgCEN1, since upon incubation of the C-terminal domain with P17-XPC a significant decrease in diameters of the particles in solution was observed (Figure 7D). These observations suggest that only the target peptide recognition at the C-terminus, which, as demonstrated above, is a key region for the high affinity interaction with P17-XPC, competes with the self-assembly process.

Discussion

The understanding of the self-assembly properties of centrins *in vitro* has been a relevant topic for several years and many studies have demonstrated that these proteins are key structural components of Ca^{2+}-sensitive filaments [17,19,44,45]. We found that TgCEN1 can self-assemble in the presence of Ca^{2+} and that the assembly process depends on different physical and chemical factors, comprising Ca^{2+} and protein concentration, temperature, ionic strength, and molecular hydrophobicity. Overall, our results support a model in which, in the presence of Ca^{2+}, both ionic and hydrophobic interactions contribute to the self-assembly of TgCEN1, in accordance with what already observed for other centrins, such as HsCEN2, HsCEN1 and EoCEN [17–19,44]. Indeed, the inhibition at high ionic strengths, and the essential role of the N-terminal region of TgCEN1 (res:

1–21), with its highly basic character, emphasize the relevance of the electrostatic component. Whereas the quenching/inhibition effect of the hydrophobic probe ANS clearly indicates that the molecular associations also have a hydrophobic character. Of interest, while at high salt concentration (150 mM KCl) TgCEN1 is monomeric in solution, the addition of ANS only partially quenched the aggregation process, suggesting that electrostatic interactions likely are the major forces driving the Ca^{2+}-dependent self-assembly behaviors of TgCEN1. Ca^{2+} requirement may play a dual function in the association process; Ca^{2+} binding to TgCEN1 caused the exposure of hydrophobic surfaces, as previously demonstrated [16], therefore supporting its hydrophobic contribution to the self-assembly. Moreover, it can enhance the interactions between neighboring centrin molecules by mediating ionic interactions.

Various mechanisms have been suggested for describing the self-association of different centrins. For HsCEN2, Craescu and coauthors favored a model in which preformed oligomers between the C-terminal domains evolve towards larger polymers via the participation of the basic N-terminal extension [17,44]. They suggested that the binding sites of the N-fragment are the negatively charged regions adjacent to the hydrophobic cavity of C-terminal domains, close to the target binding site of the centrin [17,44]. On the other hand, the self-assembly mechanism of the algal *Sherffelia dubia* centrin was that its N-terminal extension associates with the peptide-binding site of another centrin [14]. In the case of TgCEN1, the complete absence of molecular associations upon the removal of the first 21 residues, as demonstrated by both turbidity and DLS measurements, suggests that the N-terminal fragment has an essential role in protein self-association. We found that the Ca^{2+}-saturated isolated N and C domains of TgCEN1 have the propensity to form small oligomers, most likely attributable to electrostatic intermolecular interactions for the N-terminal domains and hydrophobic interactions for the C-terminal domains. However, the formation of larger final molecular particles requires the integral protein and the contribution of the basic N-terminal 21 residues which likely mediate heterologous interactions between the N- and C-terminal domains from different molecules. The ability of a 21-residue peptide, derived from the N-terminal unstructured fragment, to induce the aggregation of the truncated variant of TgCEN1 lacking the first 21 residues (Δ21TgCEN1) provide support for this hypothesis. Accordingly, the inhibition effect of the P17-XPC peptide on the association properties of the protein and of the C-terminal domain, which is a crucial recognition site for the peptide, points toward a mechanism in which the N-terminal extension of one TgCEN1 molecule may recognize and bind to a region nearby or to the peptide binding site in the C-terminus of another molecule and may be modulated by the presence of target proteins. The presence of negatively charged regions close to the peptide binding site in the C-lobe of TgCEN1 further support this mechanism (Figure 8A). However, we cannot exclude an association model in which the N-terminal domains mediate the interaction between different monomers. Recently, the crystal structure of the trimeric N-terminal domain of *Euplotes octocarinatus* centrin was reported, underpinning the ability of the protein to self-associate in a mode of N-to-N [45]. Indeed, most of the crucial residues that contribute to the forming the homotrimer in EoCen are conserved also in TgCEN1 (Supplementary Figure S6).

Clearly, the molecular associations of TgCEN1 seem to be dependent not only on the characteristics of the N-terminal extension but also on the peptide-binding site and on the interaction with potential target proteins. Interestingly, TgCEN1 displays distinct target binding properties, such as the number of binding sites, binding affinity, and sensitivity for Ca^{2+}. Titration of the peptide fragment from the human XPC protein to the intact TgCEN1 and its isolated N- and C-terminal domains revealed that the protein possesses two binding sites that interact with the peptide in a different manner. One site is in the N-terminal domain and binds P17-XPC in a strict Ca^{2+}-dependent way and with moderate affinity, while a second site is in the C-terminal domain and binds the peptide with high affinity and poor Ca^{2+} sensitivity. The ability of TgCEN1 to bind P17-XPC via the C-terminal lobe and with high affinity even in the presence of EGTA is consistent with the behaviors of many other centrins in which the C-lobe mediates the complex formation [12,35,46–50], and prompted us to propose that TgCEN1 may be constitutively bound to a target via the C-terminal lobe even at the basal level of Ca^{2+} in the cell (∼100 nM)[51]. Interestingly, residues involved in the 3D structure of the complex between HsCEN2 and P17-XPC (PDB: 2GGM, [35]) are conserved in the TgCEN1 sequence (Figure 8A).

On the other hand, the Ca^{2+} dependence of the interaction between the N-terminal domain of TgCEN1 and P17-XPC is very similar to that observed in SdCEN [20] and suggests that a Ca^{2+} stimulus can determine a second interaction with the same or different target molecules. TgCEN1 possesses two high affinity Ca^{2+}-binding sites in the N-lobe that regulate a protein conformational change [16]. The N-lobe can function as a Ca^{2+} sensor and the binding of Ca^{2+} could activate peptide recognition in the N-terminal lobe. Since TgCEN1 is mainly localized to the centrioles [15], the interaction with more targets can result in relevant dynamics and/

Biochemical Journal (2021) **478** 2571–2587
https://doi.org/10.1042/BCJ20210295

(A)

```
HsCEN2      MASNFKKANMASSSQRKRMSPKPELTEEQKQEIREAFDLFDADGTGTIDVKELKVAMRAL      60
TgCEN       -MHSRKG--ASSLPRGRGAGKKTELTEEQRQEIKEAFDLFDTDGSGCIDAKELKVAMRAL      57
SdCEN       -MS-YRK--AASARRDKAKTRSAGLTEEQKQEIREAFDLFDTDGSGTIDAKELKVAMRAL      56
                  :    :*  : :    .  *****:***:*******:**:* **.**********

HsCEN2      GFEPKKEEIKKMISEIDKEGTGKMNFGDFLTVMTQKMSEKDTKEEILKAFKLFDDDETGK      120
TgCEN       GFEPKKEEIRKMIADVDKDGTGSVDFQEFLSLMTVKMAERDPREEILKAFRLFDDDETGK      117
SdCEN       GFEPKKEEIKKMIADIDKDGSGTIDFEEFLQMMTAKMGERDSREEIMKAFRLFDDDETGK      116
            *********:***:::**:*:*.::* :** :** **.*:* :***:***:*********

HsCEN2      ISFKNLKRVAKELGENLTDEELQEMIDEADRDGDGEVSEQEFLRIMKKTSLY      172
TgCEN       ISFKNLKRVSKELGENLTDEELQEMIDEADRDGDGEINEEEFIRIMRKTNLF      169
SdCEN       ISFKNLKRVAKELGENMTDEELQEMIDEADRDGDGEVNEEEFFRIMKKTSLF      168
            *********:******:*********************.*:**:***:**.*:
```

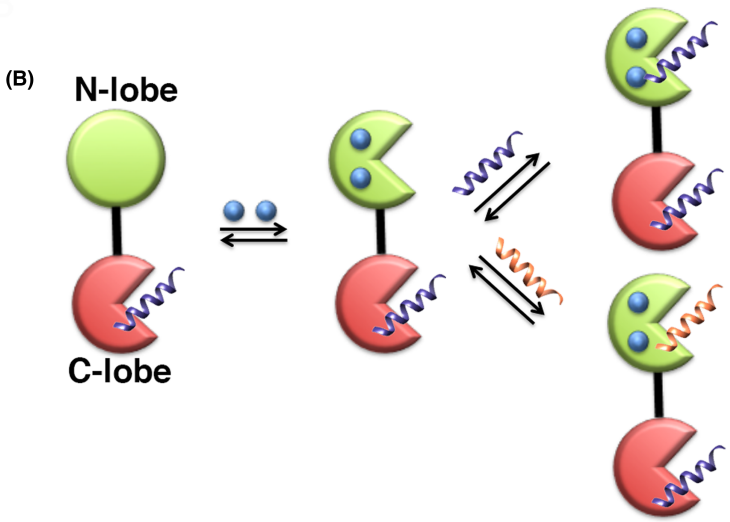

Figure 8. Sequence alignment and proposed mechanism for TgCEN1 target binding.

(**A**) Sequence alignment of the human CEN2 (HsCEN2, Uniprot: P41208) with the centrin from *S. dubia* (SdCEN, Uniprot: Q06827) and TgCEN1 (Uniprot: A0A125YHX7). Residues of HsCEN2 mainly involved in the XPC peptide binding (PDB code: 2GGM, [35]) are highlighted in yellow while acidic residues located in the XPC binding pocket are underlined. Sequences were aligned using Clustal Omega (https://www.ebi.ac.uk/Tools/msa/clustalo/) [52]. (**B**) Schematic of the target binding modes for TgCEN1 according to the data available. The N- and C-terminal domains are shown in green and red, respectively, as two types of circle representing the closed and open conformations. Ca^{2+} ions are depicted in blue.

or structural variations of local cellular assemblies with a significant impact on the structural role of the protein. Moreover, heterologous interactions involving other centrosome proteins may occur, resulting in new structural and physicochemical properties (Figure 8B).

Overall, our results suggest that an equilibrium may exist between the interaction of TgCEN1 with individual target proteins and the self-assembly propensity that would be conditioned by different parameters, such as the Ca^{2+} concentration. Of course, our experiments performed with purified TgCEN1 and a model peptide, although easier to study, represent a simplification of the possible protein–protein interactions. In this context, the identification of TgCEN1 physiological targets as well as molecular structure determination will be crucial to better describe these aspects and to understand the Ca^{2+}-controlled structural changes and function of TgCEN1 in the highly dynamic structure of centrosomes.

Data Availability

All data generated during this study are included in this article and the corresponding Supplementary File.

Competing Interests
The authors declare that there are no competing interests associated with the manuscript.

Funding
This research was supported by departmental funds provided by the Italian Ministry of Research and Education (FUR2018, FUR2019 to A.A. and P.D.) and in part by the Italian MIUR-PRIN 2017 grant No. 2017ZBBYNC (to A.A. and A.D.M.).

CRediT Author Contribution
Alessandra Astegno: Conceptualization, Supervision, Funding acquisition, Writing — original draft, Writing — review and editing. **Carolina Conter:** Conceptualization, Investigation, Writing — review and editing. **Luca Bombardi:** Investigation, Writing — review and editing. **Marco Pedretti:** Investigation, Writing — review and editing. **Filippo Favretto:** Investigation, Writing — review and editing. **Adele Di Matteo:** Funding acquisition, Investigation, Writing — review and editing. **Paola Dominici:** Funding acquisition, Writing — review and editing.

Acknowledgements
We thank the Centro Piattaforme Tecnologiche of the University of Verona for providing access to the NMR spectrometer, MicroCal PEAQ-ITC (Malvern), CD spectropolarimeter (Jasco) and Zetasizer Nano ZS instrument.

Abbreviations
CaM, calmodulin; CD, circular dichroism; DLS, dynamic light scattering; HsCEN1, human centrin 1; ITC, isothermal titration calorimetry; MTOCs, microtubule-organizing centers; NMR, Nuclear magnetic resonance spectroscopy; TEV, Tobacco Etch Virus.

References
1 Coling, D.E. and Salisbury, J.L. (1992) Characterization of the calcium-binding contractile protein centrin from Tetraselmis striata (Pleurastrophyceae). *J. Protozool.* **39**, 385–391 https://doi.org/10.1111/j.1550-7408.1992.tb01468.x
2 Huang, B., Mengersen, A. and Lee, V.D. (1988) Molecular cloning of cDNA for caltractin, a basal body-associated Ca^{2+}-binding protein: homology in its protein sequence with calmodulin and the yeast CDC31 gene product. *J. Cell Biol.* **107**, 133–140 https://doi.org/10.1083/jcb.107.1.133
3 Salisbury, J.L., Baron, A., Surek, B. and Melkonian, M. (1984) Striated flagellar roots: isolation and partial characterization of a calcium-modulated contractile organelle. *J. Cell Biol.* **99**, 962–970 https://doi.org/10.1083/jcb.99.3.962
4 Baum, P., Furlong, C. and Byers, B. (1986) Yeast gene required for spindle pole body duplication: homology of its product with Ca^{2+}-binding proteins. *Proc. Natl Acad. Sci. U.S.A.* **83**, 5512–5516 https://doi.org/10.1073/pnas.83.15.5512
5 Madeddu, L., Klotz, C., Le Caer, J.P. and Beisson, J. (1996) Characterization of centrin genes in paramecium. *Eur. J. Biochem.* **238**, 121–128 https://doi.org/10.1111/j.1432-1033.1996.0121q.x
6 Del Vecchio, A.J., Harper, J.D.I., Vaughn, K.C., Baron, A.T., Salisbury, J.L. and Overall, R.L. (1997) Centrin homologues in higher plants are prominently associated with the developing cell plate. *Protoplasma* **196**, 224–234 https://doi.org/10.1007/BF01279570
7 Paoletti, A., Moudjou, M., Paintrand, M., Salisbury, J.L. and Bornens, M. (1996) Most of centrin in animal cells is not centrosome-associated and centrosomal centrin is confined to the distal lumen of centrioles. *J. Cell Sci.* **109**, 3089–3102 https://doi.org/10.1242/jcs.109.13.3089
8 Nishi, R., Okuda, Y., Watanabe, E., Mori, T., Iwai, S., Masutani, C. et al. (2005) Centrin 2 stimulates nucleotide excision repair by interacting with xeroderma pigmentosum group C protein. *Mol. Cell. Biol.* **25**, 5664–5674 https://doi.org/10.1128/MCB.25.13.5664-5674.2005
9 Liang, L., Flury, S., Kalck, V., Hohn, B. and Molinier, J. (2006) CENTRIN2 interacts with the Arabidopsis homolog of the human XPC protein (AtRAD4) and contributes to efficient synthesis-dependent repair of bulky DNA lesions. *Plant Mol. Biol.* **61**, 345–356 https://doi.org/10.1007/s11103-006-0016-9
10 Miron, S., Durand, D., Chilom, C., Perez, J. and Craescu, C.T. (2011) Binding of calcium, magnesium, and target peptides to Cdc31, the centrin of yeast *Saccharomyces cerevisiae*. *Biochemistry* **50**, 6409–6422 https://doi.org/10.1021/bi200518d
11 Jani, D., Lutz, S., Marshall, N.J., Fischer, T., Kohler, A., Ellisdon, A.M. et al. (2009) Sus1, Cdc31, and the Sac3 CID region form a conserved interaction platform that promotes nuclear pore association and mRNA export. *Mol. Cell* **33**, 727–737 https://doi.org/10.1016/j.molcel.2009.01.033
12 La Verde, V., Trande, M., D'Onofrio, M., Dominici, P. and Astegno, A. (2018) Binding of calcium and target peptide to calmodulin-like protein CML19, the centrin 2 of *Arabidopsis thaliana*. *Int. J. Biol. Macromol.* **108**, 1289–1299 https://doi.org/10.1016/j.ijbiomac.2017.11.044
13 Pedretti, M., Conter, C., Dominici, P. and Astegno, A. (2020) SAC3B is a target of CML19, the centrin 2 of *Arabidopsis thaliana*. *Biochem. J.* **477**, 173–189 https://doi.org/10.1042/BCJ20190674
14 Wiech, H., Geier, B.M., Paschke, T., Spang, A., Grein, K., Steinkotter, J. et al. (1996) Characterization of Green alga, yeast, and human centrins. Specific subdomain features determine functional diversity. *J. Biol. Chem.* **271**, 22453–22461 https://doi.org/10.1074/jbc.271.37.22453

15 Hu, K., Johnson, J., Florens, L., Fraunholz, M., Suravajjala, S., DiLullo, C. et al. (2006) Cytoskeletal components of an invasion machine–the apical complex of *Toxoplasma gondii*. *PLoS Pathog.* **2**, e13 https://doi.org/10.1371/journal.ppat.0020013
16 Bombardi, L., Pedretti, M., Conter, C., Dominici, P. and Astegno, A. (2020) Distinct calcium binding and structural properties of two centrin isoforms from *Toxoplasma gondii*. *Biomolecules* **10**, 1142 https://doi.org/10.3390/biom10081142
17 Tourbez, M., Firanescu, C., Yang, A., Unipan, L., Duchambon, P., Blouquit, Y. et al. (2004) Calcium-dependent self-assembly of human centrin 2. *J. Biol. Chem.* **279**, 47672–47680 https://doi.org/10.1074/jbc.M404996200
18 Zhao, Y., Guo, X. and Yang, B. (2019) Calcium-induced human centrin 1 self-assembly and double-regulating the binding with peptide R18-Sfi1p. *Int. J. Biol. Macromol.* **128**, 314–323 https://doi.org/10.1016/j.ijbiomac.2019.01.096
19 Zhao, Y., Song, L., Liang, A. and Yang, B. (2009) Characterization of self-assembly of *Euplotes octocarinatus* centrin. *J. Photochem. Photobiol. B Biol.* **95**, 26–32 https://doi.org/10.1016/j.jphotobiol.2008.12.006
20 Radu, L., Durussel, I., Assairi, L., Blouquit, Y., Miron, S., Cox, J.A. et al. (2010) Scherffelia dubia centrin exhibits a specific mechanism for Ca^{2+}-controlled target binding. *Biochemistry* **49**, 4383–4394 https://doi.org/10.1021/bi901764m
21 Araki, M., Masutani, C., Takemura, M., Uchida, A., Sugasawa, K., Kondoh, J. et al. (2001) Centrosome protein centrin 2/caltractin 1 is part of the xeroderma pigmentosum group C complex that initiates global genome nucleotide excision repair. *J. Biol. Chem.* **276**, 18665–18672 https://doi.org/10.1074/jbc.M100855200
22 Gornall, A.G., Bardawill, C.J. and David, M.M. (1949) Determination of serum proteins by means of the biuret reaction. *J. Biol. Chem.* **177**, 751–766 https://doi.org/10.1016/S0021-9258(18)57021-6
23 Conter, C., Oppici, E., Dindo, M., Rossi, L., Magnani, M. and Cellini, B. (2019) Biochemical properties and oxalate-degrading activity of oxalate decarboxylase from bacillus subtilis at neutral pH. *IUBMB Life* **71**, 917–927 https://doi.org/10.1002/iub.2027
24 Trande, M., Pedretti, M., Bonza, M.C., Di Matteo, A., D'Onofrio, M., Dominici, P. et al. (2019) Cation and peptide binding properties of CML7, a calmodulin-like protein from *Arabidopsis thaliana*. *J. Inorg. Biochem.* **199**, 110796 https://doi.org/10.1016/j.jinorgbio.2019.110796
25 Astegno, A., La Verde, V., Marino, V., Dell'Orco, D. and Dominici, P. (2016) Biochemical and biophysical characterization of a plant calmodulin: Role of the N- and C-lobes in calcium binding, conformational change, and target interaction. *Biochim. Biophys. Acta Proteins Proteomics* **1864**, 297–307 https://doi.org/10.1016/j.bbapap.2015.12.003
26 Astegno, A., Giorgetti, A., Allegrini, A., Cellini, B. and Dominici, P. (2013) Characterization of C-S Lyase from *C. diphtheriae*: a possible target for new antimicrobial drugs. *Biomed. Res. Int.* **2013**, 701536 https://doi.org/10.1155/2013/701536
27 Vallone, R., La Verde, V., D'Onofrio, M., Giorgetti, A., Dominici, P. and Astegno, A. (2016) Metal binding affinity and structural properties of calmodulin-like protein 14 from *Arabidopsis thaliana*. *Protein Sci.* **25**, 1461–1471 https://doi.org/10.1002/pro.2942
28 Rossi, P., Xia, Y., Khanra, N., Veglia, G. and Kalodimos, C.G. (2016) (15)N and (13)C- SOFAST-HMQC editing enhances 3D-NOESY sensitivity in highly deuterated, selectively [(1)H,(13)C]-labeled proteins. *J. Biomol. NMR* **66**, 259–271 https://doi.org/10.1007/s10858-016-0074-5
29 Astegno, A., Bonza, M.C., Vallone, R., La Verde, V., D'Onofrio, M., Luoni, L. et al. (2017) Arabidopsis calmodulin-like protein CML36 is a calcium (Ca^{2+}) sensor that interacts with the plasma membrane Ca^{2+}-ATPase isoform ACA8 and stimulates its activity. *J. Biol. Chem.* **292**, 15049–15061 https://doi.org/10.1074/jbc.M117.787796
30 Delaglio, F., Grzesiek, S., Vuister, G.W., Zhu, G., Pfeifer, J. and Bax, A. (1995) NMRPipe: a multidimensional spectral processing system based on UNIX pipes. *J. Biomol. NMR* **6**, 277–293 https://doi.org/10.1007/BF00197809
31 Vranken, W.F., Boucher, W., Stevens, T.J., Fogh, R.H., Pajon, A., Llinas, M. et al. (2005) The CCPN data model for NMR spectroscopy: development of a software pipeline. *Proteins* **59**, 687–696 https://doi.org/10.1002/prot.20449
32 Kozlowski, L.P. and Bujnicki, J.M. (2012) Metadisorder: a meta-server for the prediction of intrinsic disorder in proteins. *BMC Bioinformatics* **13**, 1–11 https://doi.org/10.1186/1471-2105-13-111
33 Popescu, A., Miron, S., Blouquit, Y., Duchambon, P., Christova, P. and Craescu, C.T. (2003) Xeroderma pigmentosum group C protein possesses a high affinity binding site to human centrin 2 and calmodulin. *J. Biol. Chem.* **278**, 40252–40261 https://doi.org/10.1074/jbc.M302546200
34 Charbonnier, J.B., Renaud, E., Miron, S., Le Du, M.H., Blouquit, Y., Duchambon, P. et al. (2007) Structural, thermodynamic, and cellular characterization of human centrin 2 interaction with xeroderma pigmentosum group C protein. *J. Mol. Biol.* **373**, 1032–1046 https://doi.org/10.1016/j.jmb.2007.08.046
35 Thompson, J.R., Ryan, Z.C., Salisbury, J.L. and Kumar, R. (2006) The structure of the human centrin 2-Xeroderma pigmentosum group C protein complex. *J. Biol. Chem.* **281**, 18746–18752 https://doi.org/10.1074/jbc.M513667200
36 Latham, M.P., Zimmermann, G.R. and Pardi, A. (2009) NMR chemical exchange as a probe for ligand-binding kinetics in a theophylline-binding RNA aptamer. *J. Am. Chem. Soc.* **131**, 5052–5053 https://doi.org/10.1021/ja900695m
37 Favretto, F., Flores, D., Baker, J.D., Strohaker, T., Andreas, L.B., Blair, L.J. et al. (2020) Catalysis of proline isomerization and molecular chaperone activity in a tug-of-war. *Nat. Commun.* **11**, 6046 https://doi.org/10.1038/s41467-020-19844-0
38 Ikura, M., Clore, G.M., Gronenborn, A.M., Zhu, G., Klee, C.B. and Bax, A. (1992) Solution structure of a calmodulin-target peptide complex by multidimensional NMR. *Science* **256**, 632–638 https://doi.org/10.1126/science.1585175
39 Meador, W.E., Means, A.R. and Quiocho, F.A. (1992) Target enzyme recognition by calmodulin: 2.4 A structure of a calmodulin-peptide complex. *Science* **257**, 1251–1255 https://doi.org/10.1126/science.1519061
40 Popescu, S.C., Popescu, G.V., Bachan, S., Zhang, Z., Seay, M., Gerstein, M. et al. (2007) Differential binding of calmodulin-related proteins to their targets revealed through high-density Arabidopsis protein microarrays. *Proc. Natl Acad. Sci. U.S.A.* **104**, 4730–4735 https://doi.org/10.1073/pnas.0611615104
41 Astegno, A., Maresi, E., Marino, V., Dominici, P., Pedroni, M., Piccinelli, F. et al. (2014) Structural plasticity of calmodulin on the surface of CaF2 nanoparticles preserves its biological function. *Nanoscale* **6**, 15037–15047 https://doi.org/10.1039/C4NR04368E
42 Hoeflich, K.P. and Ikura, M. (2002) Calmodulin in action: diversity in target recognition and activation mechanisms. *Cell* **108**, 739–742 https://doi.org/10.1016/S0092-8674(02)00682-7
43 Shi, E., Zhang, W., Zhao, Y. and Yang, B. (2017) Modulation of XPC peptide on binding Tb^{3+} to *Euplotes octocarinatus* centrin. *Metallomics* **9**, 1796–1808 https://doi.org/10.1039/C7MT00263G
44 Yang, A., Miron, S., Duchambon, P., Assairi, L., Blouquit, Y. and Craescu, C.T. (2006) The N-terminal domain of human centrin 2 has a closed structure, binds calcium with a very low affinity, and plays a role in the protein self-assembly. *Biochemistry* **45**, 880–889 https://doi.org/10.1021/bi051397s

45 Wang, W., Zhao, Y., Wang, H. and Yang, B. (2018) Crystal structure of the trimeric N-terminal domain of ciliate *Euplotes octocarinatus* centrin binding with calcium ions. *Protein Sci.* **27**, 1102–1108 https://doi.org/10.1002/pro.3418
46 Martinez-Sanz, J., Yang, A., Blouquit, Y., Duchambon, P., Assairi, L. and Craescu, C.T. (2006) Binding of human centrin 2 to the centrosomal protein hSfi1. *FEBS J.* **273**, 4504–4515 https://doi.org/10.1111/j.1742-4658.2006.05456.x
47 Hu, H. and Chazin, W.J. (2003) Unique features in the C-terminal domain provide caltractin with target specificity. *J. Mol. Biol.* **330**, 473–484 https://doi.org/10.1016/S0022-2836(03)00619-3
48 Hu, H., Sheehan, J.H. and Chazin, W.J. (2004) The mode of action of centrin: binding of Ca^{2+} and a peptide fragment of Kar1p to the C-terminal domain. *J. Biol. Chem.* **279**, 50895–50903 https://doi.org/10.1074/jbc.M404233200
49 Azimzadeh, J., Hergert, P., Delouvée, A., Euteneuer, U., Formstecher, E., Khodjakov, A. et al. (2009) hPOC5 is a centrin-binding protein required for assembly of full-length centrioles. *J. Cell Biol.* **185**, 101–114 https://doi.org/10.1083/jcb.200808082
50 Jani, D., Lutz, S., Hurt, E., Laskey, R.A., Stewart, M. and Wickramasinghe, V.O. (2012) Functional and structural characterization of the mammalian TREX-2 complex that links transcription with nuclear messenger RNA export. *Nucleic Acids Res.* **40**, 4562–4573 https://doi.org/10.1093/nar/gks059
51 Pace, D.A., McKnight, C.A., Liu, J., Jimenez, V. and Moreno, S.N. (2014) Calcium entry in *Toxoplasma gondii* and its enhancing effect of invasion-linked traits. *J. Biol. Chem.* **289**, 19637–19647 https://doi.org/10.1074/jbc.M114.565390
52 Madeira, F., Park, Y.M., Lee, J., Buso, N., Gur, T., Madhusoodanan, N. et al. (2019) The EMBL-EBI search and sequence analysis tools APIs in 2019. *Nucleic Acids Res.* **47**, W636–W641 https://doi.org/10.1093/nar/gkz268

SUPPLEMENTARY MATERIAL

The interplay of self-assembly and target binding in centrin 1 from *Toxoplasma gondii*

Carolina Conter[1†], Luca Bombardi[1†], Marco Pedretti[1], Filippo Favretto[1], Adele Di Matteo[2], Paola Dominici[1], Alessandra Astegno[1*]

[1] Department of Biotechnology, University of Verona, Strada Le Grazie 15, 37134 Verona, Italy.

[2] Institute of Molecular Biology and Pathology, CNR, Piazzale Aldo Moro, 5, 00185 Rome, Italy.

†These authors contributed equally to the work.

*Corresponding author: Alessandra Astegno, e-mail: alessandra.astegno@univr.it

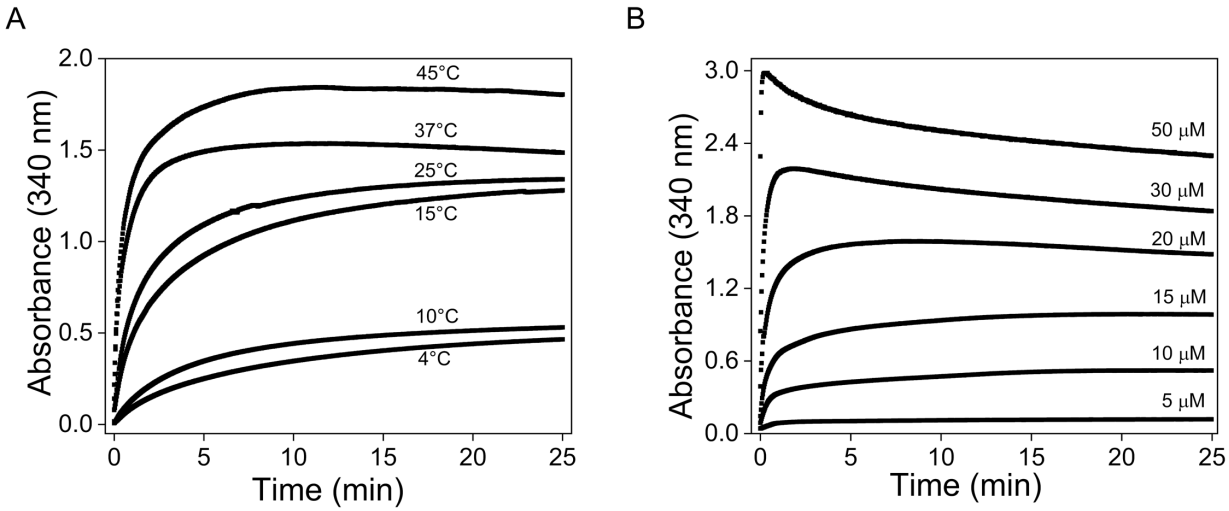

Figure S1. Effect of temperature and protein concentration on TgCEN1 Ca^{2+}-dependent self-assembly. Light scattering (measured as the turbidity at 340 nm) as a function of time at given temperature and protein concentrations for the samples in 20 mM Tris–HCl, 20 mM KCl pH 7.5 and with 1 mM $CaCl_2$ at 37 °C.

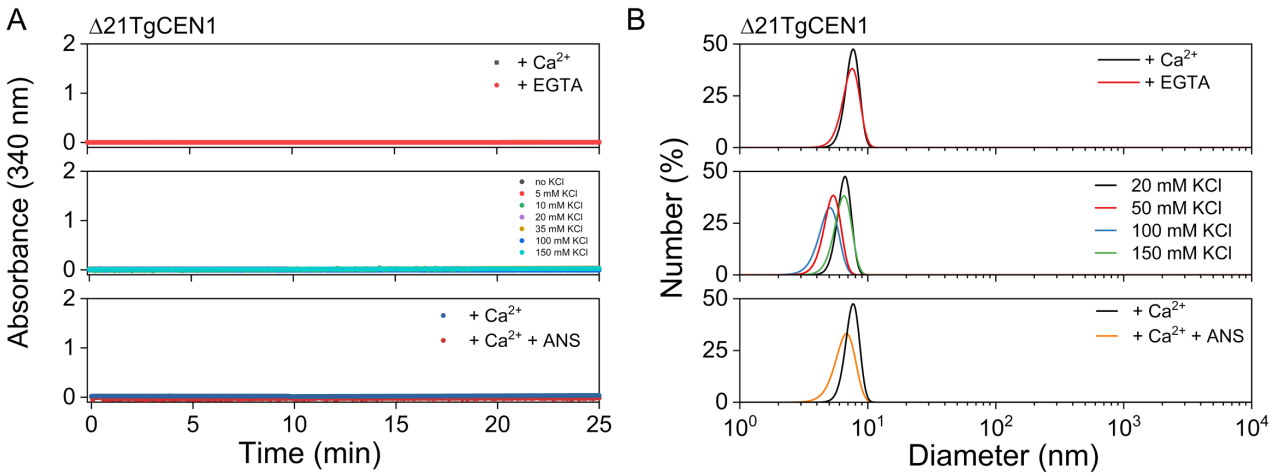

Figure S2. Light scattering experiments of Δ21TgCEN1. (A) Scattering intensity (measured as the turbidity at 340 nm) and (**B**) particle-size distribution from DLS data of Δ21TgCEN1 at 37°C in 20 mM Tris–HCl, 20 mM KCl pH 7.5 in the presence of 1 mM $CaCl_2$ or 1 mM EGTA (top), at selected KCl concentrations in the presence of 1 mM $CaCl_2$ (middle), and upon addition of 600 µM ANS in the presence of 1 mM $CaCl_2$ (bottom).

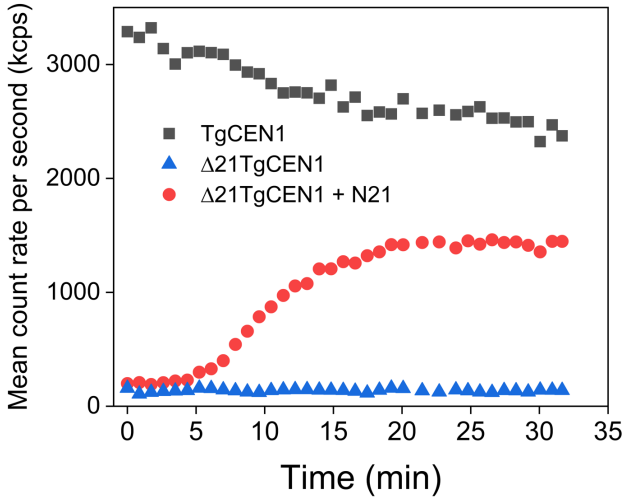

Figure S3. Time-dependent changes of the DLS total count rate (measured as kilocounts per second) of Δ21TgCEN1 before (blue line) and upon (red line) addition of 50 µM N21 peptide in the presence of 1 mM $CaCl_2$. The profile of intact TgCEN1 (black line) was also reported.

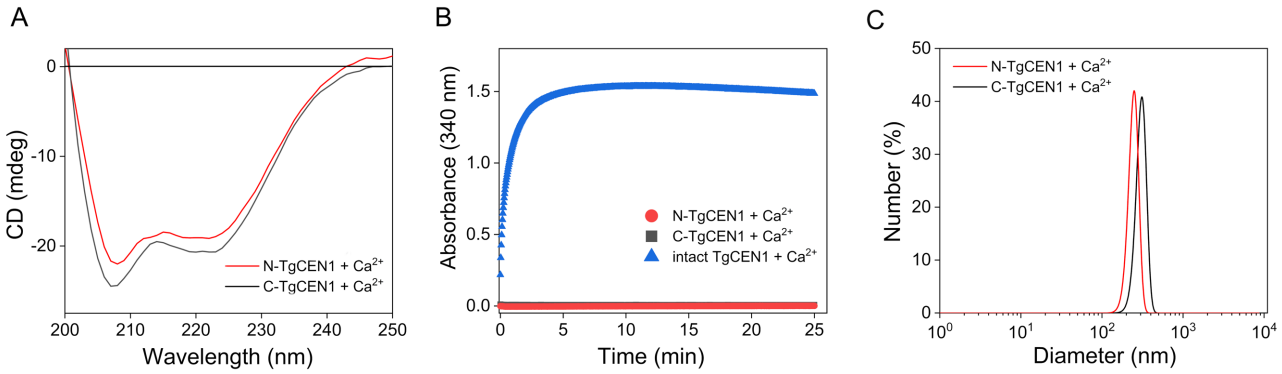

Figure S4. Far-UV CD spectra (A), turbidity profiles (B) and DLS (C) spectra of the isolated domains N-TgCEN1 and C-TgCEN1 in the presence of 1 mM $CaCl_2$. (**A**) Far-UV CD spectra of 20 µM N-TgCEN1 (red line) and C-TgCEN1 (black line) in the presence of 1 mM $CaCl_2$. (**B**) Turbidity measurements of 20 µM N-TgCEN1 (red) and C-TgCEN1 (black) measured at 340 nm as a function of time in 20 mM Tris–HCl, 20 mM KCl pH 7.5 at protein concentration of 20 µM, at 37°C in the presence of 1 mM $CaCl_2$. The profile of intact TgCEN1 (blue) is also shown. (**C**) Particle-size distribution from DLS data of 10 µM N-TgCEN1 (red line) and C-TgCEN1 (black line) in 20 mM Tris–HCl, 20 mM KCl pH 7.5, 1 mM $CaCl_2$.

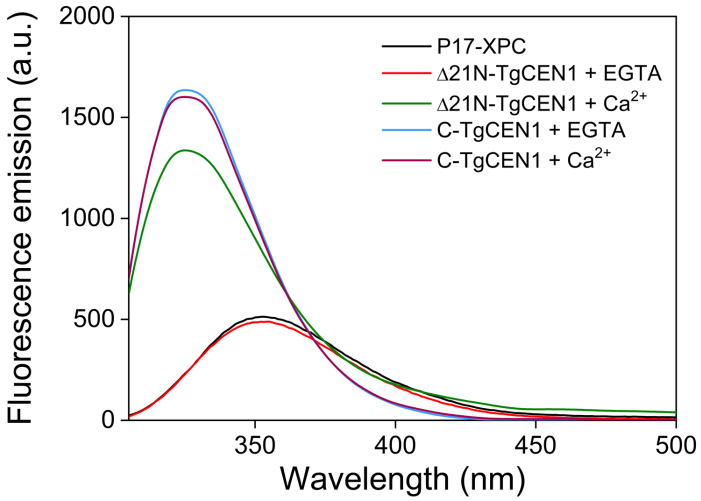

Figure S5. Fluorescence analysis of P17-XPC binding to the isolated domains. Complex formation monitored by Trp fluorescence in the presence of $CaCl_2$ or EGTA. Trp fluorescence emission spectra of 5 µM P17-XPC alone (black), and upon addition of stoichiometric concentration of C-TgCEN1 in the presence of $CaCl_2$ (purple) or EGTA (light blue) or upon addition of stoichiometric concentration of Δ21N-TgCEN1 in the presence of $CaCl_2$ (green) or EGTA (red).

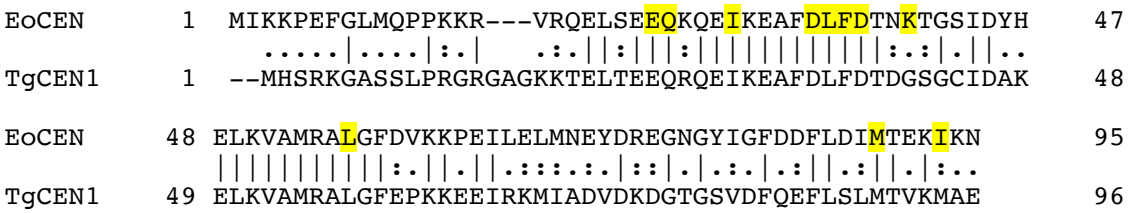

Figure S6. Sequence alignment of the N-terminal domain of centrin 1 from *T. gondii* (TgCEN1, Uniprot: A0A125YHX7) with the centrin from *E. octocarinatus* (EoCEN, Uniprot: Q9XZV2). Residues involved in intermolecular interaction in the crystal structure of the trimeric N-EoCEN (PDB code: 5Z1Q, [1]) are highlighted in yellow. Sequences were aligned using Emboss needle service (https://www.ebi.ac.uk/Tools/psa/emboss_needle/) [2].

References

1. Wang, W., et al., *Crystal structure of the trimeric N-terminal domain of ciliate Euplotes octocarinatus centrin binding with calcium ions.* Protein Science, 2018. **27**(6): p. 1102-1108.
2. Madeira, F., et al., *The EMBL-EBI search and sequence analysis tools APIs in 2019.* Nucleic Acids Res, 2019. **47**(W1): p. W636-w641.